A Computational Investigation of Multi-Rotor Interactional Aerodynamics with Hub Lateral and Longitudinal Canting

Richard Healy PhD Student
Farhan Gandhi Redfern Professor
Center for Mobility with Vertical Lift (MOVE), Rensselaer Polytechnic Institute, New York, USA

Mihir Mistry Ridley Park, PA
Michael Duffy St. Louis, MO
The Boeing Company

ABSTRACT

This study investigates the interactional aerodynamics for laterally and longitudinally canted two rotor systems with a front rotor and an aft rotor aligned with the flow. The 5.5 ft, 3 bladed fixed pitched rotors are simulated using CFD at a targeted $5lb/ft^2$ disk loading and 30 kts. Simulations are performed using the commercial Navier Stokes solver AcuSolve with a detached eddy simulation (DES) model. In addition to an uncanted case, two laterally canted cases (10° advancing sides up and 10° advancing sides down) as well as two longitudinally canted cases (10° inward and 10° outward) are simulated. Aft rotor performance is compared to isolated rotors operating at the same RPM, speed and shaft tilt angle in order to quantify the effect of rotor-rotor aerodynamic interaction. For all configurations, the aft rotors experience a lift deficit at the front of the rotor disk which also results in a nose down pitching moment relative to an isolated rotor. The lift deficit for the uncanted rotor was around 15%. Lateral canting only slightly increases the lift deficit (to 16-17%) but also produces 28-38% change in roll moments. Change in nose-up pitching moments for the uncanted and laterally canted rotors were in the 55%-64% range. Longitudinal canting produces larger changes in the magnitude of the lift deficit and pitching moment, but has minimal effect on roll moments. In particular, canting inward results in a lift deficit as high as 21% and a 94% change in pitching moment. Canting outward, on the other hand, reduces the aft rotor lift deficit to 11% and the pitching moment change to 19%. The paper explains the changes in the flow field and the underlying physics for the different cases in detail.

INTRODUCTION

Over the last few year, there has been a huge interest in large electric multi-rotor aircraft (eVTOL aircraft) for Urban Air Mobility (for example, as described in the Uber Elevate vision and the NASA UAM Grand Challenge), commercial package delivery, and military/law-enforcement applications. The current batteries powering most of these eVTOL aircraft exhibit very low energy density relative to hydrocarbon fuels used by larger convectional VTOL aircraft. With this limitation, it is especially important to maximize the aerodynamic performance of eVTOL aircraft in order to realize practical payload capacity, endurance and range (factors not so important to previous hobbyist and recreational users). One area that requires particular attention is the understanding of the interactional aerodynamic effects of rotors operating in close proximity and their impact on performance.

A number of recent studies have used Computational Fluid Dynamics (CFD) to simulate and understand the complex flows associated with interactional aerodynamics of rotors operating in close proximity. Researchers at the NASA Advanced Supercomputing Division have used CFD to simulate large and small-scale quadcopters in hover and forward flight. Yoon et al. (Ref. 1) investigated the effects of rotor separation for an XV-15 derivative quadcopter in hover, and observed up to a 4% decrease in rotor efficiency for rotors in close proximity. At the smaller scale, Yoon et al. simulated the Straight Up Imaging (SUI) Endurance quad-copter at 10 m/s cruise speed (Ref. 2) and reported a 28% thrust deficit on the aft rotors when compared to the front rotors. Other work by Diaz and Yoon (Ref. 3) found that vertical rotor separation via over/under mounting influenced rotor interaction on a quadcopter in cruise. Misiorowski, Gandhi and Oberai also used CFD to simulate quadcopters operating in cruise in the plus and cross configurations (Ref. 4), and provided physical insights into the difference in interactional aerodynamics for the two configurations. CFD simulations of in-line large UAM scale rotors in cruise by Healy, Misiorowski and Gandhi (Ref. 5) were used to systematically examine the effects of vertical and longitudinal rotor spacing on interactional aeordynamic effects.

Whereas the studies above have simulated multi-rotor configurations with uncanted rotors, many modern eVTOL designs

Presented at the VFS International 76th Annual Forum & Technology Display, Virginia Beach, Virginia, USA, October 6–8, 2020.

are incorporating canted rotors (where the axis of rotation is inclined from the vertical, Fig. 1) in an effort to realize benefits that include improved yaw authority (Refs. 6, 7, 8). The present study looks to quantify the effects of lateral and longitudinal rotor cant on interactional aeorydnamics for a large UAM-scale 2-rotor system in cruise. The CFD simulations use the commercial Navier-Stokes solver AcuSolve, previously used in Refs. 4 and 5 with two rotors aligned in the direction of flight, and differential lateral and longitudinal cant introduced on the rotors. This study also focuses on examining the underlying physical phenomena behind the differences in behavior for the different canted cases.

Figure 1. Laterally canted rotors on the Boeing PAV (Ref. 9)

ANALYSIS

Two in-line fixed-pitch rotors in forward flight are simulated using CFD. The front rotor spins clockwise and the aft rotor spin counterclockwise at the same rotational speed. Rotor hubs are positioned in-line with the free-stream as many large UAM utilize a dedicated propeller for propulsion. In particular, the rotor hubs are positioned with 2.5R longitudinal separation, and no vertical separation. However, while the position of the rotors is held constant, the relative shaft tilt angle, or cant of each rotor is varied. For lateral canting, both rotors are set at zero pitch attitude relative to the flow, and rotated in the roll direction. Three configurations are shown in Fig. 2: uncanted, 10° cant with the advancing sides up, and 10° cant with the advancing sides down. In contrast, for longitudinal canting, both rotors are counter-rotated in the pitch direction. Fig. 3 compares uncanted, 10° cant inward, and 10° cant outward cases.

The rotors used have a 5.5ft diameter, with specifications detailed in Table 1. A CAD image of the rotor is shown in Fig. 4. The Rensselaer Multirotor Analysis Code (RMAC) (Ref. 10), based on blade element theory (BET) with 3x4 finite state Peters-He inflow representation is used to evaluate an appropriate root pitch and RPM for a target 5 $\frac{\text{lb}}{\text{ft}^2}$ disk loading in hover. A 20° root pitch, and 1600 RPM is found to provide sufficiently power and hover tip Mach number. CFD simulations are performed at 30kts forward speed, which represents a $\mu = 0.1$ advance ratio.

Table 1. Rotor Parameters

Parameter	Specification
Diameter	5.5 ft
Number of Blades	3
Solidity	0.076
Root Cutout	0.2R
Airfoil	NACA 23012
Twist	−10°
Planform	Rectangular
Chord	6.56 in
Root Pitch	20°
RPM	1600 RPM
Hover Tip Mach No.	0.41

All simulations are conducted using the commercial Navier-Stokes solver AcuSolve which uses a stabilized 2nd order upwind finite element method. AcuSolve simulations for an SUI Endurance rotor were previously shown to compare well against experimental results (Ref. 4). For a 2-rotor unit, the computational domain is shown in Fig. 5. The nonrotating volume is a rectangular prism with sides at least 25 rotor radii away from the front rotor hub. The front and top boundaries are set to the freestream velocity, while the sides, bottom and back are set to outflow with backflow conditions enabled, which allows for flow in either direction across the boundary with zero pressure offset. Around each rotor is a cylindrical rotating volume with radius 1.06 rotor radii and extending two tip chord lengths above and below the rotor plane. Each surface of the cylindrical rotating volumes have a sliding mesh interface which passes information to and from the non-rotating volume that comprises the remainder of the computational domain.

The domain is discretized using an entirely unstructured, tetrahedral mesh. On each blade, the surface mesh is set to ensure 200 elements around the airfoil countour, with refinement along the leading and trailing edges ($0-10\%$ and $90-100\%$ chord respectively). A portion of the blade surface mesh is shown in Fig. 6. The boundary layer in the wall-normal direction is highly resolved, with the first element height set to ensure a $y+ < 1$. The boundary layer is grown until the last layer size is within 80% of the local off-body element size, and is shown in Fig. 7. Around the rotors (1R above and below), a wake refinement region is defined in which the element size is prescribed as $\frac{1}{4}$ tip chord. Below and downstream of the rotor plane, a second refinement region is prescribed with elements $\frac{1}{1}$ tip chord in size. This second refinement region is skewed back in order to capture the rotor wake as it convects downstream (Fig. 8). The entire computational domain is comprised of 120 million elements, with 48 million in each rotating volume, and 24 million in the surrounding non-rotating volume. A mesh refinement study was performed in which the surface mesh size, edge refinement, boundary layer, and wake refinement were doubled independently. For the mesh used in the simulations, the thrust and torque changed by less than 2% and 3% respectively when compared to the finer meshes.

A detached eddy simulation (DES) is used with the Spalart-

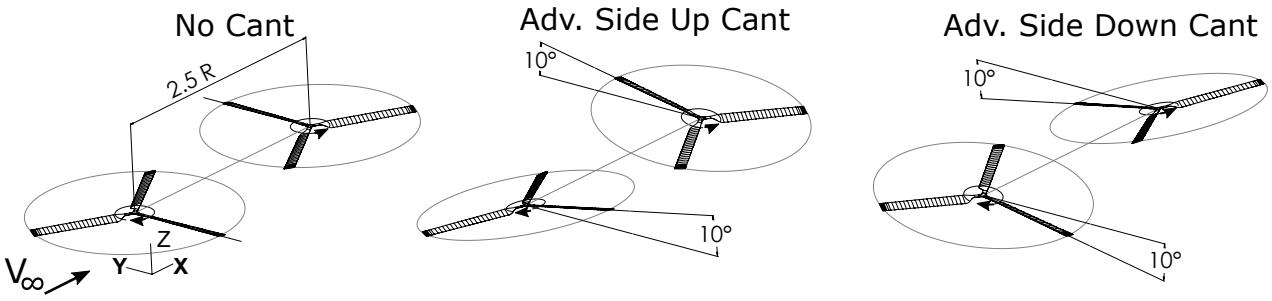

Figure 2. Two-rotor system for uncanted, advancing side up, and advancing side down cant cases

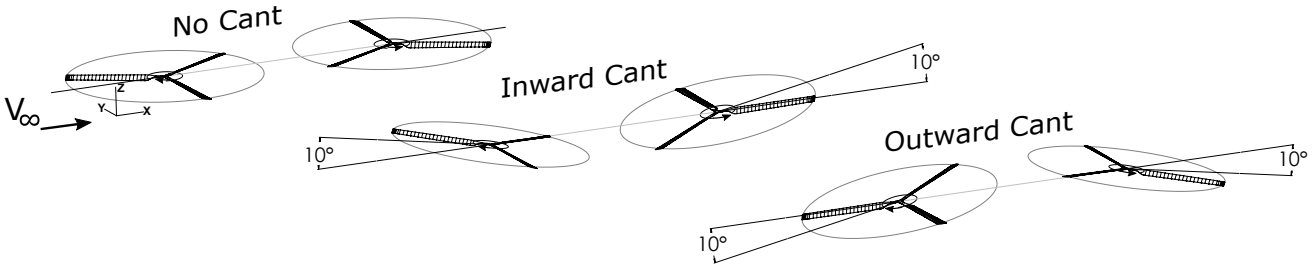

Figure 3. Two-rotor system for uncanted, canted inward, and canted outward cases

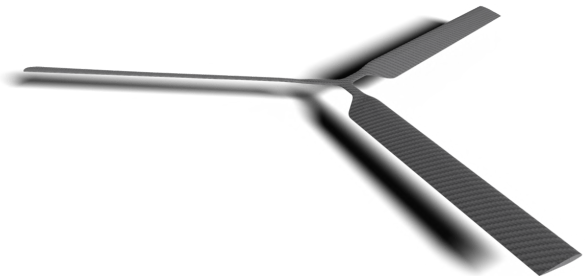

Figure 4. Rotor CAD

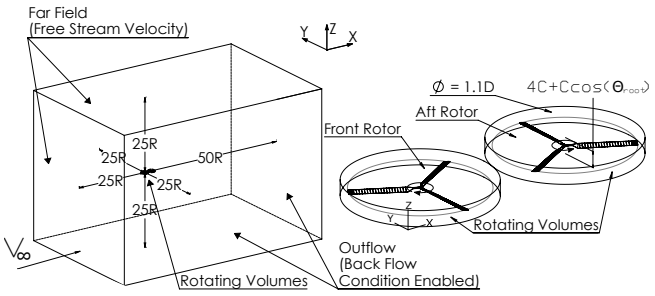

Figure 5. Diagram of the computational domain

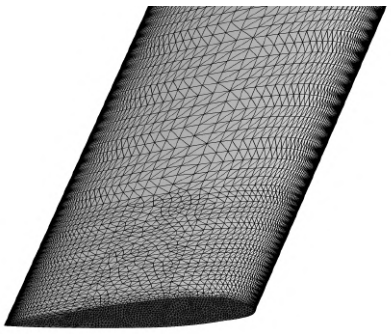

Figure 6. Blade surface mesh viewed near the blade tip

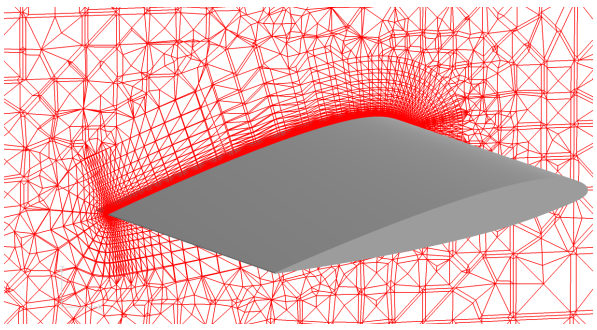

Figure 7. Blade surface mesh viewed near the blade tip

Allmarus (SA) turbulence model for all simulations. Each case is initially run using time steps corresponding to 10° of rotation for at least 40 revolutions in order to reduce the computational cost of rotor wake development. These initial 10° time steps are possible without numerical divergence due to the stability afforded by the Streamline Upwind Petrov-Galerkin (SUPG) stabilized finite element method and generalized α implicit time integration method. The latter method was designed to suppress high frequency distrubances and allow solution stability with Courant-Friedrichs-Lewy (CFL) number greater than 1 (Refs 11, 12). Following the revolutions simulated with 10° time steps, an additional 3 revolutions are performed with time steps corresponding to 1°. Three revolutions is sufficient time to allow air at the front rotor to travel downstream of the aft rotor. All runs are performed on 512 2.6GHz Intel Xeon E5-2650 processors, part of the Center for Computational Innovations (CCI) at Rensselaer Polytechnic Institute.

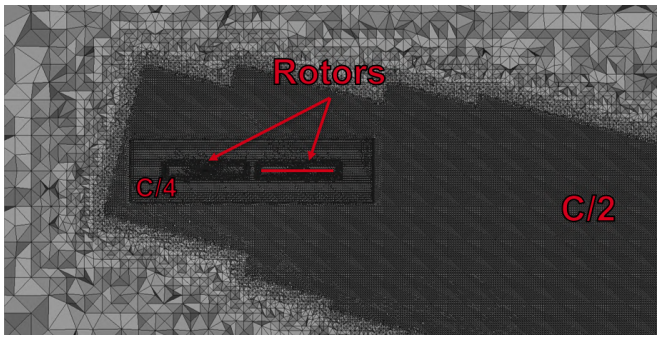

Figure 8. Cross-section of wake mesh refinement

RESULTS

Uncanted Rotor Performance

An isolated counterclockwise rotor in 30 kts nose-level flight is simulated at 1600 RPM. This condition represents how the aft rotor in an uncanted 2-rotor system would perform in the absence of a front rotor. Figure 9 shows the sectional thrust coefficient (dC_T/dx) for the isolated rotor with flow moving from left to right. Relatively higher thrust is produced on the advancing side between $\psi = 90^o$ and 135^o. This observation is consistent with that seen in Ref. 4 and is caused by higher dynamic pressure on the advancing side of the rotor, in conjunction with longitudinal inflow variation (Ref. 13).

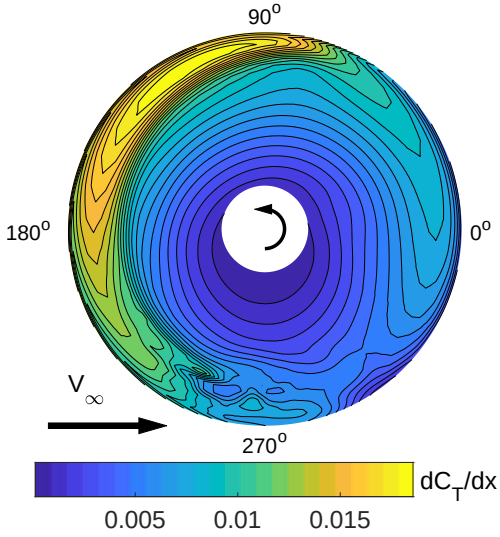

Figure 9. Sectional thrust coefficient, dCt/dx, for isolated rotor

An uncanted two rotor system is first simulated to identify the interactional aerodynamic effects. Figure 10 shows the sectional thrust coefficient (dC_T/dx) for an uncanted two rotor system, again in 30 kts nose-level flight at 1600 RPM. The front rotor for this case shows nearly identical performance characteristics to an isolated clockwise rotor, indicating the aft rotor in this system has little effect on the front rotor. In contrast, the aft rotor exhibits a smaller area of high thrust, which lies farther back on the rotor disk (around $\psi = 90°$) when compared to the isolated rotor case in Fig. 9 (high lift centered around $\psi = 110°$, and extending past $\psi = 150°$). By comparing isolated and aft rotor loads in this way, the affect of interactional aerodynamics can be extracted.

Uncanted/Laterally Canted Front Rotor Wake Aerodynamics

The difference in aft rotor thrust distribution compared to the isolated case can be explained through investigation of the front rotor wake convection. Figure 11 shows induced vertical (Z) velocity averaged over 1 revolution on 3 planes cutting through the location of an uncanted aft rotor disk (no aft rotor actually simulated). Iso-surfaces of Q-criterion colored by x-vorticity are also shown. In the region between the advancing and retreating side rollup vortices, strong downwash is observed on the three planes cutting through the location of the aft rotor disk (outlined in magenta). Looking at the middle slice, the aft rotor disk is positioned above the vortex rollup, and above the strongest downwash. However, on the front slice (A:A), the front of the disk intersects the top extremity of the darkest blue, corresponding to the strongest downwash region.

Fig. 12 shows slice A:A from Fig. 11 as viewed from the rear. Here, the uncanted rotor is seen to lie at the top of the strong downwash region. However, when the rotors are canted with the advancing sides up, the aft rotor's retreating side is positioned closer to the front rotor's advancing side rollup vortex. This close proximity causes the aft rotor's retreating side to interact with areas of higher downwash. On the advancing side, the canted aft rotor is positioned further away from the front rotor's retreating side rollup vortex, away from the strongest downwash. With the rotors canted with advancing sides down, the reverse is observed. The aft rotor disk's retreating side is positioned relatively farther away from the front rotor's advancing side rollup vortex, out of the downwash. Conversely, its advancing side is positioned in close proximity to the retreating side rollup vortex, moving into the region of strong downwash.

The effects of rotor cant on downwash and upwash over the entire aft rotor disk can be observed in Fig. 13. This figure shows the rev-averaged velocity normal to the aft rotor plane induced by an isolated front rotor, plotted over the region that would be occupied by an aft rotor (no aft rotor actually simulated). Iso-surfaces of Q-criterion are also shown, colored by x-vorticity. For the uncanted case, downwash is strongest at the front of the aft rotor disk. The downwash reduces towards the aft of the disk as the front rotor's wake convects downwards, away from the disk and its influence weakens. Outside of the front rotor wake, upwash is induced. The wake is observed to convect laterally towards the front rotor's advancing side, causing the advancing tip of the aft rotor disk to lie outside of the front rotor wake. As a result, the advancing side of the uncanted disk experiences front rotor wake induced upwash effect in its tip region.

For the advancing side up cant, the greater lateral drift of the front rotor wake relative to the aft rotor puts a larger section of

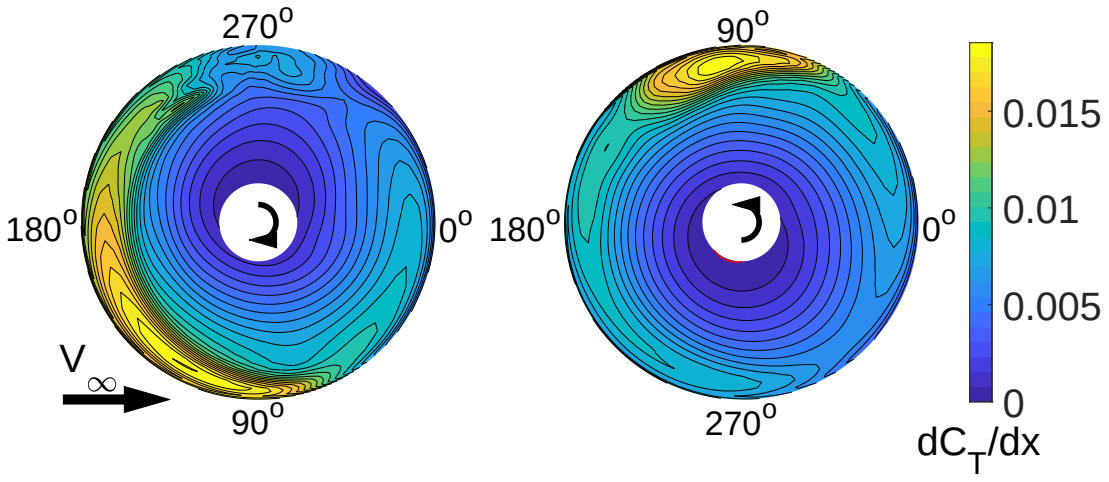

Figure 10. Sectional thrust coefficient, dCt/dx, for an uncanted two rotor system

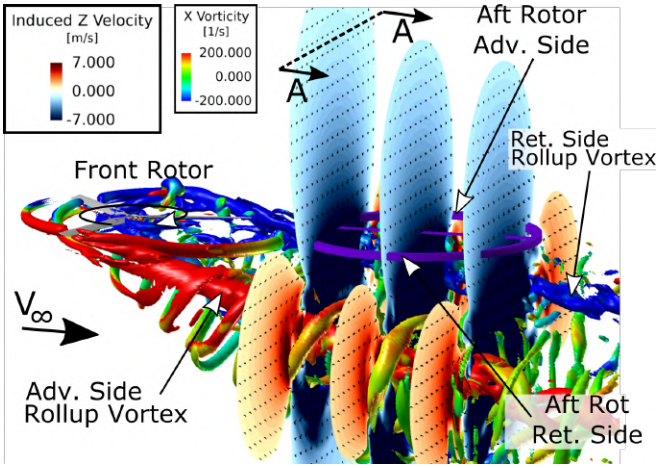

Figure 11. Velocity induced by the front rotor on the area occupied by an uncanted aft rotor

the aft rotor disk's advancing side in the upwash of the front rotor's retreating side rollup vortex. However, as seen in Fig. 13 (middle), the magnitude of this upwash is lower than the uncated case due to increased vertical separation between the front rotor retreating side rollup vortex and rear rotor disk's lifted up advancing side (Fig. 12). In Fig. 13 (middle), the retreating side of the aft rotor sees a heavy downwash due to the greater proximity of the aft disk's retreating side to the front rotor's advancing side rollup vortex (Fig. 12).

For the advancing side down cant, the lateral drift of the front rotor's wake is in the opposite direction and the aft rotor's retreating tip region does not see downwash (Fig. 13, right). The advancing side's close proximity to the front rotor's retreating side rollup vortex (Fig. 12) produces the strongest downwash over the aft rotor's advancing side (Fig. 13 right).

Impact of Lateral Cant on Rotor Thrust and Torque

The downwash and upwash induced on the aft rotor disk seen in Fig. 13 are primary contributors to the differences in thrust distribution on the aft rotor. Fig. 14 shows the difference in sectional thrust coefficient between the aft rotor in a 2 rotor system and an isolated rotor operating in identical conditions, but in the absence of a front rotor. For the uncanted rotors, strong downwash on the front of the aft rotor disk leads to a loss in lift on the front. Downwash on a blade section increases the local inflow angle, reducing the blade's angle of attack and thus its lift. On the advancing side of the disk (around $\psi = 90°$), upwash from the front rotor's retreating side rollup vortex is shown to produce a region of increased lift. Overall, an uncanted aft rotor is found to produce 15% less thrust than an isolated rotor. The canted case with advancing sides up exhibits a larger region of lift loss on the front retreating side (compare the regions around $\psi = 270°$ between uncanted and advancing side up canted cases in Fig. 14). This is a result of the stronger retreating side downwash observed in Fig. 13. Additionally, the peak lift loss observed on the uncanted rotor at $\psi = 120°$ is less dramatic for this canted case as it sees relatively less downwash in this region. On the advancing side, a larger region of thrust increase, but a lower maximum increase is observed. This is consistent with the larger region of upwash, but lower upwash magnitude as seen in Fig. 13. The integrated thrust for the advancing side up aft rotor is 17% less than an equivalent rotor in isolation. For rotor cant with advancing sides down, the low downwash on the retreating side of the aft rotor disk (seen in Fig. 12) results in minimal lift difference over this region ($\psi = 210°$ to $\psi = 240°$). However, the strong downwash on the advancing side of the disk results in significant loss in lift at about $\psi = 120$ deg. Lift deficit in this region is greater than that seen on the uncanted case due to the canted aft rotor's closer proximity to the front rotor's retreating side rollup vortex (seen in Fig. 12). Overall, the advancing side down aft rotor exhibits a 16% thrust deficit compared to an isolated rotor in the same operating conditions.

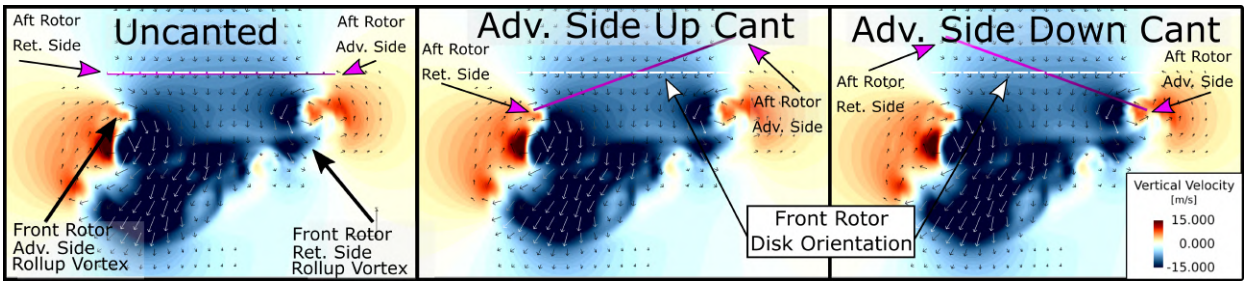

Figure 12. Slice A:A from Fig. 11 viewed from behind

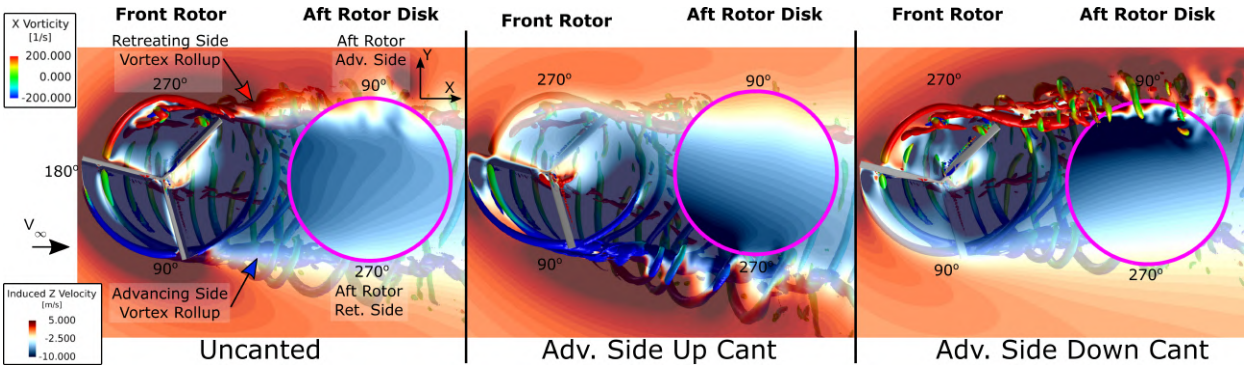

Figure 13. Front rotor induced velocity normal to the aft rotor disk in the region of the aft rotor disk as well as Q-Criterion (7500) of isolated rotor wake colored by vorticity in the freestream direction

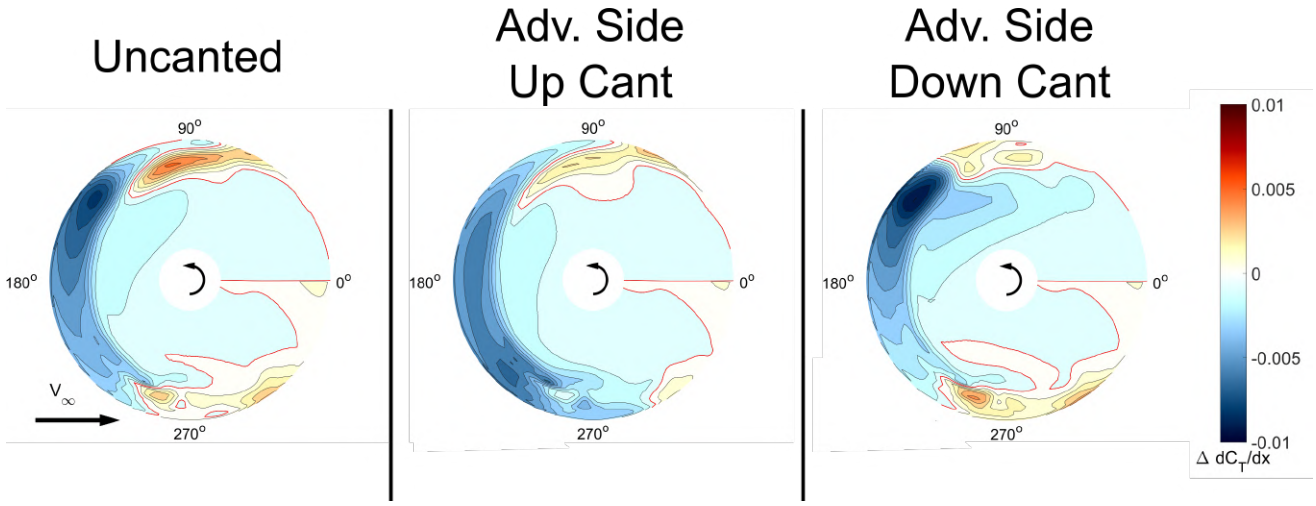

Figure 14. Sectional thrust coefficient difference, $\Delta dC_T/dx$ (aft rotor thrust minus isolated rotor thrust)

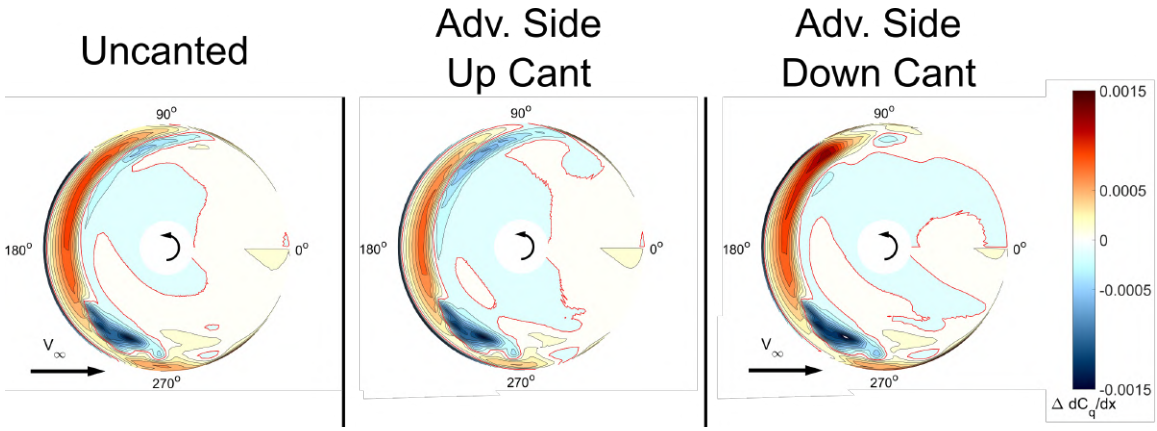

Figure 15. Sectional torque coefficient difference, $\Delta dC_q/dx$ (aft rotor torque minus isolated rotor torque)

The changes in interactional aerodynamics brought about by lateral cant also influence the torque on the aft rotor. Fig. 15 presents the difference in sectional torque coefficient between the aft rotor in a 2 rotor system, and an isolated rotor. For all cases, downwash on the front of the rotor disk leads to an increase in torque in this area. Downwash on a blade element decreases the local angle of attack, tilting the lift vector backward, increasing induced drag. The aft rotor with advancing side up displays a weaker torque penalty on the front advancing side (around $\psi = 90^\circ$ to $\psi = 135^\circ$) compared to the uncanted case. As with lift loss, this reduction in torque penalty corresponds to the lesser downwash observed in this region in Fig. 13. Overall, the advancing side up aft rotor produces 1% less torque than an isolated rotor, while the uncanted aft rotor produces 4% more. The opposite is true of the advancing side down case, where a greater torque penalty compared to the uncanted case is observed around $\psi = 130^\circ$ due to the stronger downwash observed in that region in Fig. 13. In total, the advancing side down rotor produces 5% greater torque than a rotor in isolation.

For every lateral cant case, a region of significant torque reduction is observed at about $\psi = 230^\circ$. This feature is a result of blade vortex interaction (BVI) on an isolated rotor in these operating conditions. This is due to BVI related torque increase observed over that region on the isolated rotor that is absent under the changed aerodynamic environment of the aft rotors with a front rotor present. When BVI is not observed on the isolated rotor (as with other, high disk loading cases that were simulated but have not been included in this paper), the localized regions of torque reduction seen in Fig. 15 are absent. Additionally in this case, the major observation of torque increase at the front of the aft rotor disk (for all three cases) skewing slightly to the retreating side for the advancing side up case and to the retreating side for the advancing side down case is more clearly observed.

Longitudinal Cant of an Isolated Rotor

Longitudinal rotor cant impacts rotor thrust and torque in two ways. First, longitudinal cant changes the angle of attack of the rotor relative to the freestream, leading to an effective climb (if nose down) or descent (if nose up). Second, the relative positioning of the rotors and the convection of the front rotor wake influences the interactional aerodynamics of the aft rotor. Fig. 16 quantifies the first type of thrust change by plotting the difference in rotor thrust between an isolated nose down rotor and an uncanted isolated rotor (nose down minus uncanted). This represents how changing just the relative angle of attack influences a canted inward aft rotor's thrust. The canted inward aft rotor is positioned nose down, leading to a component of freestream velocity acting downward relative to the aft rotor. This downwash over the rotor disk leads to a loss in lift as indicated by the large predominantly blue region in Fig. 16. Overall, the nose down rotor produces 9.3% less lift than an uncanted isolated rotor.

Fig. 17 presents the difference between thrust generated by a nose up isolated rotor, and that generated by an uncanted isolated rotor. This represents the change in thrust brought about by the angle of the aft rotor in a canted outward system. Here, a component of freestream acts upward on the rotor disk. The upwash through the rotor disk leads to an increase in thrust, as indicated by the white, yellow and orange regions in Fig. 17. Integrated over the disk, an 8.8% lift increase is observed for a nose up rotor.

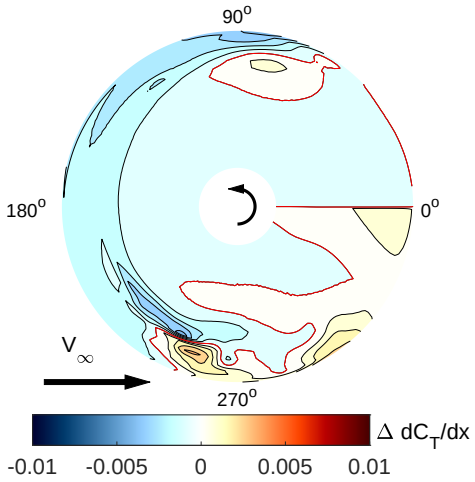

Figure 16. Sectional thrust coefficient difference, $\Delta dC_t/dx$ (isolated nose down thrust minus isolated uncanted rotor thrust)

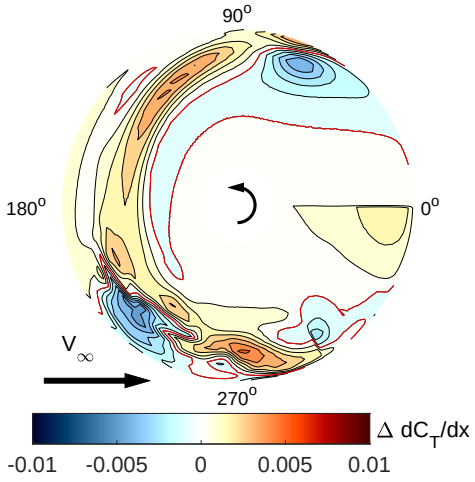

Figure 17. Sectional thrust coefficient difference, $\Delta dC_t/dx$ (isolated nose up thrust minus isolated uncanted rotor thrust)

Longitudinal canting of an isolated rotor also influences the torque. Fig. 18 shows the difference in torque between an isolated nose down rotor, and an isolated uncanted rotor. Downwash over the rotor disk is observed to increase torque, particularly over the front of the disk. Fig. 19 shows the difference in torque between an isolated nose up rotor and an isolated uncanted rotor. Upwash through the rotor disk generally reduces torque due to reduction in induced drag. Indeed, a reduction in drag is observed over much of the rotor disk.

On the nose down rotor, a region of torque reduction is seen at approximately $\psi = 230^\circ$ where BVI is observed on an iso-

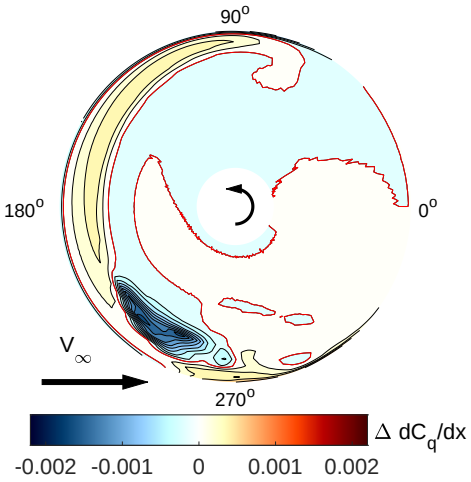

Figure 18. Sectional torque coefficient difference, $\Delta dC_q/dx$ (isolated nose down torque minus isolated uncanted rotor torque)

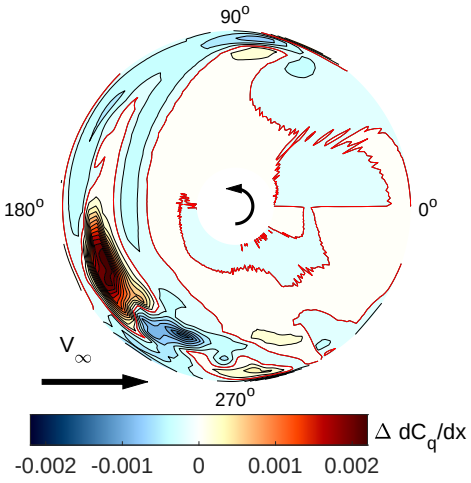

Figure 19. Sectional torque coefficient difference, $\Delta dC_q/dx$ (isolated nose up torque minus isolated uncanted rotor torque)

lated uncanted rotor. BVI is not present on the nose down rotor, leading to a relative torque reduction. On the nose up rotor, however, strong BVI is found due to the freestream velocity pushing blade tip vortices produced at the front of the disk back into the disk plane. Strong BVI at about $\psi = 210°$ is seen to produce a region of high torque.

Longitudinal Cant Aerodynamics

Longitudinal cant changes the position of the aft rotor relative to the front rotor wake. Fig. 20 shows the vertical velocity for isolated uncanted, nose up and nose down rotors over a slice cutting through the rotor hub as viewed from the left. The position of the front rotor, and the aft rotor disk (no aft rotor simulated) are also shown in pink. For each case, downwash is observed downstream of the front rotor, however, the position of the aft rotor modifies how much downwash it experiences. The uncanted aft rotor disk lies above the strongest downwash, but still intersects some darker blue towards the front. The aft rotor in the canted inward case is positoned nose down, causing the disk to intersect the strongest downwash. In contrast, the aft rotor in the canted outward case is positioned, up and consequently does not observe very strong downwash.

The impact rotor position has on the downwash observed by longitudinally canted aft rotors, as previewed in Fig. 20, can be observed over the whole aft rotor disk in Fig. 21. As with Fig. 13, a pink circle outlines the position occupied by an aft rotor disk. The interior of the pink circle is colored by velocity normal to the aft rotor plane. The uncanted aft rotor experiences stronger downwash on the front of the rotor disk, which dissipates towards the aft of the disk. The canted inward aft rotor observes yet stronger downwash near the front, as a result of its nose residing closer to the front rotor wake. However, relatively little downwash is observed over the canted outward aft rotor disk, as its nose is positioned higher up and away from the front rotor wake.

Interaction Aerodynamic Impact of Longitudinal Cant on Thrust and Torque

The differences in downwash distribution over the longitudinally canted aft rotor disks influences their thrust generation and torque requirement due to the presence of the front rotor. Fig. 22 presents the thrust difference between uncanted and longitudinally canted aft rotors, and isolated rotors in the same operating conditions: uncanted aft minus uncanted isolated (left), canted-in aft minus isolated nose down (middle), canted-out aft minus isolated nose up (right). These comparisons identify how changes in longitudinal canting impact interactional aerodynamics, excluding changes brought about by changing the rotors' angle of attack. Due to its strong downwash over the front of the rotor disk, the canted-in aft rotor (middle) loses the most lift at the front. The lift loss is greater than that observed for an uncanted aft rotor (left). The canted-out aft rotor (right), however, observes relatively little downwash over the front of the disk, leading to a smaller lift loss overall.

As with thrust, differences in interactional aerodynamics also impacts torque. Fig. 23 shows the aft rotor torque difference between uncanted and longitudinally canted aft rotors, and their respective isolated rotor counterparts. Overall, downwash on the front of the disks tends to increase torque. The canted inward aft rotor is found to produce less of a torque increase on the front of the disk than the uncanted case. Despite the stronger downwash in this area, this could potentially be due to the substantial lift loss reducing induced drag. On the canted out aft rotor, although minimal downwash is induced on the disk, equitable levels of torque increase to the uncanted case are observed. It is possible that the relatively higher lift compared to the uncanted aft rotor produces greater induced drag.

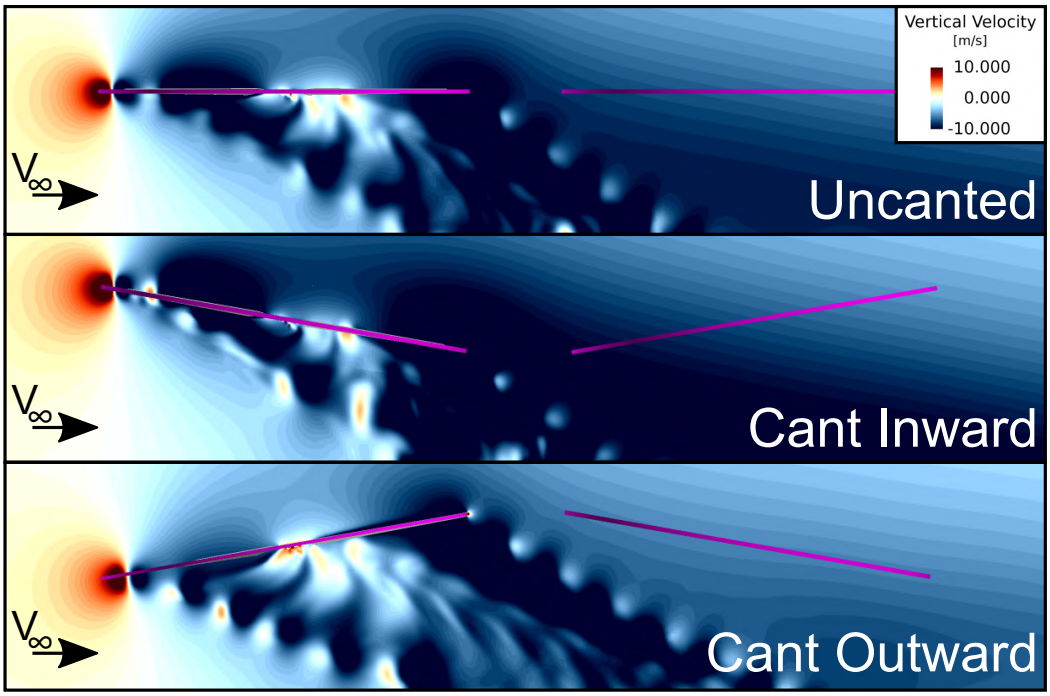

Figure 20. Vertical velocity generated by isolated uncanted, nose up and nose down rotors over a slice cutting through the rotor hub as viewed from the side

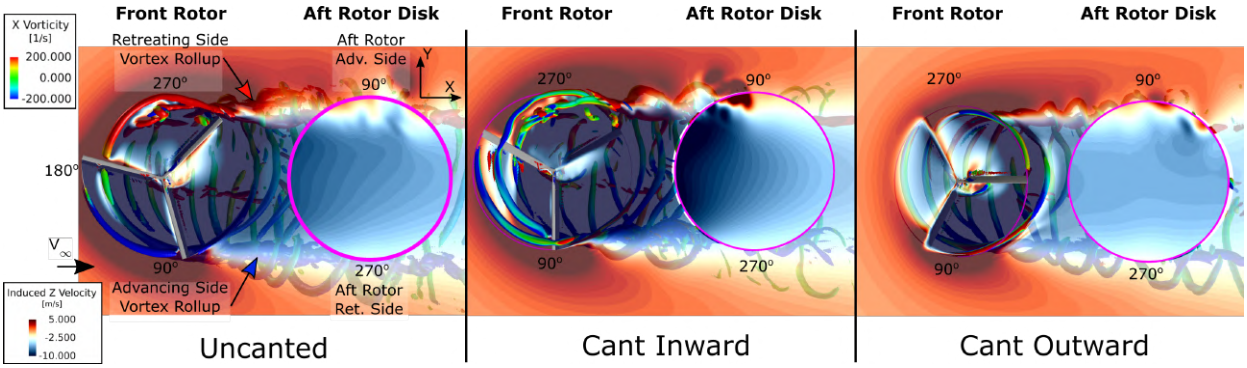

Figure 21. Vertical velocity generated by isolated uncanted, nose up and nose down rotors over the aft rotor disk location as viewed from above. Iso surfaces of Q-Criterion colored by vorticity in the downstream direction are also included

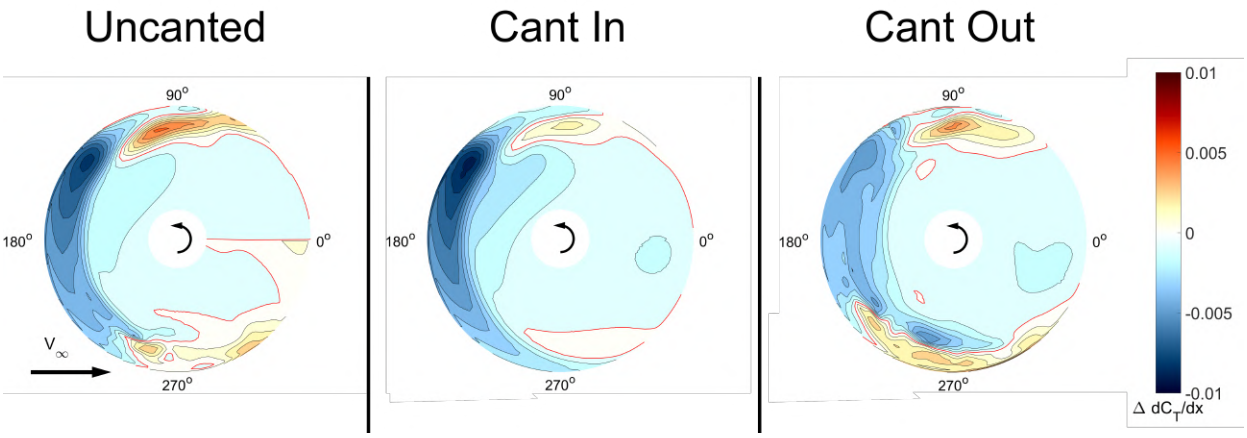

Figure 22. Sectional thrust coefficient difference, $\Delta dC_t/dx$ (aft rotor thrust minus isolated rotor thrust)

No localized region of torque reduction is present on the cant in case as the isolated nose down rotor does not experience significant BVI. In contrast, the canted-out aft rotor does show a region of torque reduction centered around $\psi = 225^\circ$. While the isolated nose up rotor produces BVI, the aft nose up rotor in the cant-out configuration does not.

Table 2 summarizes the effects longitudinal canting has on thrust and torque due to changing the rotor's angle of attack, as well as due to interactional aerodynamic differences. Columns ΔT_α and ΔQ_α denote changes in thrust and torque due to changing the rotor's angle of attack. Columns ΔT_{aero} and ΔQ_{aero} represent changes in thrust and torque due purely to interactional aerodynamics by comparing to longitudinally canted isolated rotors. Columns ΔT_{total} and ΔQ_{total} give total differences in thrust and torque between longitudinally canted aft rotors, and an isolated uncanted rotor. The canted inward aft rotor loses some thrust due to angle of attack, however a majority of its 26% thrust deficit is brought about by interactional aerodynamics. For the canted-out aft rotor, while some thrust improvement is gained by being angled nose up, interactional aerodynamics still lead to a moderate 4% thrust deficit. Compared to the uncanted case, the low degree of interactional aerodynamics, coupled with the thrust improvement from upwash leads to a relatively small deficit overall.

Integrated torque is also impacted by longitudinal canting. The canted inward aft rotor has a net torque penalty of 2% primarily due to interactional aerodynamics. The canted outward aft rotor has a net torque reduction of under 1% mainly due to the torque reduction associated with a rearward tilted aft rotor.

Integrated Loads Comparison

Table 3 reports the changes in aft rotor thrust and hub moments (relative to the corresponding thrust and moments generated when the same rotor is operating in isolation) for all five cases in this study (uncanted, advancing side up and advancing side down lateral cant, and inward and outward lateral cant). The aft rotor thrust deficit for the two laterally canted cases (advancing side up and advancing side down) is observed to be generally similar (17% and 16% respectively), and only slightly higher than the thrust deficit for the uncanted aft rotor (15%). The two longitudinally canted cases, on the other hand, produce vastly different thrust deficits (11% for canted outward, and 21% for canted inward). Clearly, the canted outward configuration does better than the uncated configuration, while the canted inward configuration does substantially worse. The change in torque for all configurations is observed to be well under 5%.

For the uncanted and longitudinally canted rotors, since there was no dramatic lateral skew of the aft rotor lift deficit, the change in roll moment (relative to the rotor operating in isolation) is small and is observed to be in the 3-11% range. Lateral canting, on the other hand, skews the aft rotor lift deficit to the advancing or retreating side (Fig. 14) to produce much larger changes in roll moment (28-38%) than those observed for the uncanted and longitudinally canted cases. For the advancing side up lateral cant, the lift deficit skews to the retreating side to produce a roll-left moment change relative to the rotor operating in isolation. Conversely, for advancing side down cant, the lift deficit skews to the advancing side, to instead produce a roll-right moment change.

With the aft rotor lift deficit always occurring at the front of the disk, this results in a net nose-down moment change for all five cases (relative to rotors operating in isolation). Since the uncanted and laterally canted configurations generally experience similar aft rotor lift deficits, the net nose-down pitching moments are also comparable (55-64%). On the other hand, with vastly differing lift deficits observed for the longitudinally canted cases, the changes in pitching moments show a wide variation as well. For the inward cant, where the aft rotor had the largest lift deficit, the change in pitching moment is as high as 94%. For the outward cant, where the aft rotor had the most modest lift deficit, the change in pitching moment is only 19%.

CONCLUSIONS

This study investigates the impact of lateral and longitudinal rotor canting on interactional aerodynamics for counter-rotating rotors positioned in-line with the flow. The computational fluid dynamics code AcuSolve, with Detached Eddy Simulation, was used to simulated airflow through the system. The sliding mesh method was used to simulate blade motion by interfacing two rotating volumes (one for each rotor) within a nonrotating volume. Every simulation was performed with 5.5 ft diameter, 3 bladed rotors with uniform planform and linearly twisted blades spining at 1600 RPM, corresponding to a 5 $\frac{lb}{ft^2}$ target disk loading. In all, five two-rotor cases were simulated: uncanted, 10° lateral cant with advancing sides up, 10° lateral cant with advancing sides down, 10° longitudinal cant inward, and 10° longitudinal cant outward. Additional isolated rotor cases were also simulated, corresponding to each of the aft rotors' operating conditions. These isolated rotor simulations were used to quantify the thrust and moment differences between aft and isolated rotors. Through these simulations, the following observations were made.

1. Regardless of the cant orientation, the front rotor's wake induces downwash on the aft rotor, leading to a decrease in thrust generation. Downwash (and as a result, lift deficit) is most predominantly observed on the front of the aft rotor disk due to downward front rotor wake convection with longitudinal distance. Lift deficit on the front of the rotor disk leads to a nose down pitching moment relative to a rotor in isolation.

2. An uncanted aft rotor is positioned above the front rotor's advancing and retreating side rollup vortices, and avoids the strongest downwash generated by the front rotor. However, when the aft rotor is laterally canted with advancing side up, its retreating side moves closer to the

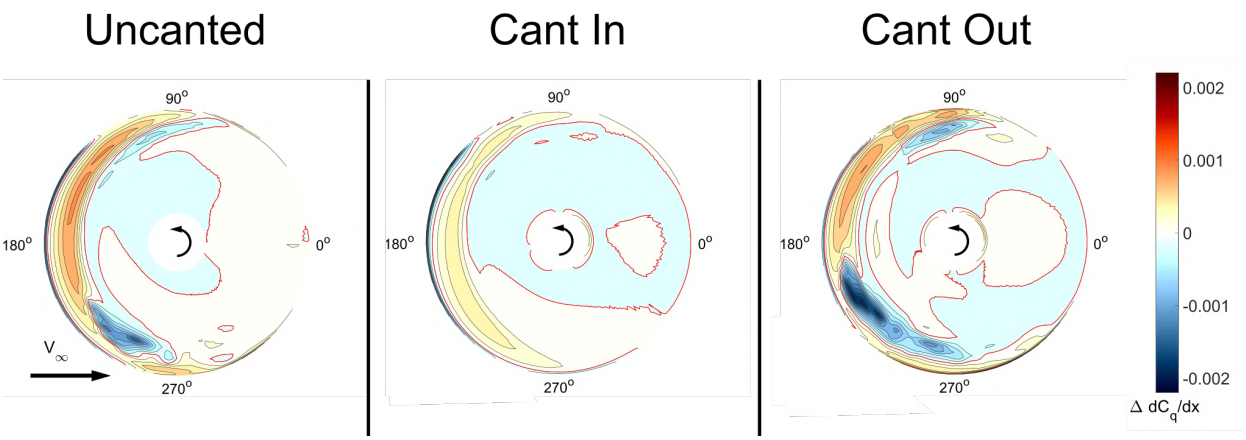

Figure 23. Sectional torque coefficient difference, $\Delta dC_q/dx$ (aft rotor torque minus isolated rotor torque)

Table 2. Longitudinal cant thrust and torque breakdown

Configuration	ΔT_α	ΔT_{aero}	ΔT_{total}	ΔQ_α	ΔQ_{aero}	ΔQ_{total}
Uncanted	0.0%	-14.7%	-14.6%	0.0%	4.4%	4.4%
Cant Inward	-5.5%	-21.2%	-25.6%	-0.5%	2.7%	2.2%
Cant Outward	8.0%	-11.2%	-4.1%	-2.2%	1.6%	-0.7%

front rotor's advancing side rollup vortex where downwash is strong. Stronger downwash on the retreating side of the disk skews the lift deficit on the front of the rotor towards the retreating side which also results in a roll left moment relative to the isolated rotor. In contrast, when the aft rotor is laterally canted with advancing side *down*, it is the advancing side that moves closer to the front rotor's retreating side rollup vortex. In this case, it is the advancing side that observes the greatest downwash. This skews the lift deficit towards the advancing side which results in a roll right moment relative to the isolated rotor.

3. Longitudinally canting the rotors inwards results in the front of the nose down aft rotor sitting close to the front rotor wake, within strong downwash. Strong downwash over the front of the rotor disk leads to high thrust penalties, higher than that observed on an uncanted aft rotor. High thrust penalties on the front of the disk results in strong nose down pitching moment relative to an isolated rotor. Longitudinally canting outwards, however, positions the front of the nose up aft rotor away from the front rotor wake. With the front of the disk out of the strongest downwash, only moderate thrust penalties are observed. When only moderate thrust penalties are present, the nose down moment relative to an isolated rotor is also small.

4. Thrust penalties for uncanted and laterally canted aft rotors are moderate, ranging from 15 to 17%. Moderate thrust penalties correspond to moderate changes in pitching moment (55-64%). Longitudinally canting the rotors, however, dramatically modifies the thrust penalty. Canting inward increases the lift deficit to as high as 21% which corresponds to a 95% change in pitching moment. Canting outward reduces the lift deficit to 11% and the pitching moment to 19%. Overall, changes in torque are less than 5%. The change in rolling moment for uncanted and longitudinally canted rotors are moderate. However, laterally canted rotors modify the roll moment by up to 28-38%.

ACKNOWLEDGMENTS

We would like to acknowledge the support of Boeing for this project, and the technical input of Boeing engineers David Mason, Ted Meadowcroft, Roger Lacy, Rachel Nelson and Mori Mani.

REFERENCES

1. S. Yoon, H. C. Lee, and T. H. Pulliam, "Computational Analysis of Multi-Rotor Flows," in *AIAA 54th Aerospace Sciences Meeting, San Diego, CA, USA*, Jan. 2016.

2. S. Yoon, P. V. Diaz, D. D. Boyd Jr., W. M. Chan, and C. R. Theodore, "Computational aerodynamic modeling of small quadcopter vehicles," in *Proceedings of the 73rd Annual Forum*, (Fort Worth), AHS International, May 2017.

3. P. Ventura Diaz and S. Yoon, "High-Fidelity Computational Aerodynamics of Multi-Rotor Unmanned Aerial Vehicles," AIAA SciTech Forum, American Institute of Aeronautics and Astronautics, Oct. 2018.

4. M. Misiorowski, F. Gandhi, and A. A. Oberai, "Computational study on rotor interactional effects for a

Table 3. Integrated thrust and torque difference between canted aft rotors and corresponding isolated rotors operating in the same operating conditions

Case	Thrust	Torque	Roll Moment	Pitch Moment
Uncanted	-14.7%	4.4%	-9.6%	-63.9%
Adv. Side Up	-17.4%	-0.7%	28.1%	-61.3%
Adv. Side Down	-15.9%	4.5%	-37.7%	-55.1%
Canted Inward	-21.2%	2.7%	-11.0%	-94.1%
Canted Outward	-11.2%	1.6%	3.1%	-18.9%

quadcopter in edgewise flight," *AIAA Journal*, 2019. https://doi.org/10.2514/1.J058369.

5. R. Healy, M. Misiorowski, and F. Gandhi, "A Systematic CFD-Based Examination of Rotor-Rotor Separation Effects on Interactional Aerodynamics for Large eVTOL Aircraft," in *Proceedings of the 75th Annual Forum*, (Philadelphia), VFS International, May 2019.

6. B. Phillips, V. Hrishikeshavan, D. Yeo, and I. Chopra, "Experimental Evaluation of a Quadrotor Biplane with Variable Pitch Rotors," in *American Helicopter Society 73rd Annual Forum, Fort Worth, TX*, AHS, May 2017.

7. Aurora Flight Sciences, "PAV - Passenger Air Vehicle," 2019. https://www.aurora.aero/pav-evtol-passenger-air-vehicle/.

8. R. Niemiec and F. Gandhi, "Effect of rotor cant on trim and autonomous flight dynamics of a quadcopter," in *Proceedings of the 74th Annual Forum*, (Phoenix), AHS International, May 2018.

9. Mztourist, "Boeing passenger air vehicle mockup at dubai air show 2019." https://commons.wikimedia.org/w/index.php?curid=84237925, Nov. 2019. Own work, CC BY-SA 4.0,.

10. R. Niemiec and F. Gandhi, "Development and Validation of the Rensselaer Multicopter Analysis Code (RMAC): A Physics-Based Low-Fidelity Modeling Tool," in *75th Annual Forum of the Vertical FLight Society*, (Philadelphi), 2019.

11. K. E. Jansen, C. H. Whiting, and G. M. Hulbert, "A generalized-alpha method for integrating the filtered navier-stokes equations with a stabilized finite element method," 2000.

12. A. N. Brooks and T. J.R. Hughes, "Streamline Upwind/Petrov-Galerkin Formulations for Convection Dominated Flows with Particular Emphasis on the Incompressible Navier-Stokes Equations," *Computer Methods in Applied Mechanics and Engineering*, vol. 32, pp. 199–259, 09 1982.

13. R. Niemiec, *Development and Application of a Medium-Fidelity Analysis Code for Multicopter Aerodynamics and Flight Mechanics*. PhD thesis, Rensselaer Polytechnic Institute, August 2018.